PCCP

Tritium Adsorption and Absorption on (100) and (001) Surfaces of Pure and Tin Defective Zirconium

Journal:	*Physical Chemistry Chemical Physics*
Manuscript ID	CP-ART-01-2025-000215.R1
Article Type:	Paper
Date Submitted by the Author:	10-Mar-2025

Complete List of Authors:	Redington, Morgan; National Energy Technology Laboratory; University at Buffalo, Chemistry Paudel, Hari; National Energy Technology Laboratory, Functional Materials Engineering Tafen, De Nyago; National Energy Technology Laboratory Miller, Daniel; Hofstra University, Chemistry Zurek, Eva; University at Buffalo, Chemistry Duan, Yuhua; National Energy Technology Laboratory

ARTICLE

Tritium Adsorption and Absorption on (100) and (001) Surfaces of Pure and Tin Defective Zirconium

Received 00th January 20xx,
Accepted 00th January 20xx

DOI: 10.1039/x0xx00000x

Morgan Redington[a,b], Hari P. Paudel[a,c], De Nyago Tafen[a,d], Daniel P. Miller[e], Eva Zurek[b], and Yuhua Duan[a,*]

Zirconium alloys such as Zircaloy-4 are used as tritium (T) getter materials in tritium-producing burnable absorber rods (TPBARs) due to their ability to capture T, thereby forming metal hydrides. Developing an understanding of T adsorption onto Zircaloy prior to diffusion into the subsurface is relevant for rational tritium getter and TPBAR design, to improve material properties for nuclear applications. Herein, density functional theory calculations revealed the preferred binding sites for T adsorption on Zr(001) and Zr(100). The energy barriers of T transfer, along the surface and from the surface to the subsurface were computed. The adsorption properties of Zr(001) were found to be superior to those of Zr(100). Surface tin impurities were found to strongly repel T. The presence of subsurface and surface tin resulted in higher absorption energy barriers for both the forward and reverse processes. Based on the calculated energy barriers, a surface to surface T diffusion coefficient of 9.53 x 10^{-10} m^2s^{-1} is expected for pristine Zr(001). A surface to subsurface T diffusion coefficient on the order of 10^{-13} m^2s^{-1} is predicted in pristine Zr, decreasing to 10^{-19} m^2s^{-1} for the transfer with a subsurface tin impurity.

Introduction

Zirconium (Zr) alloys, such as zircaloy-4, are materials utilized for their ability to capture hydrogen species and their isotopes, such as tritium (T), which chemisorb to them thereby forming metal hydrides.[1-3] These metal hydrides can then be treated to release the stored T, allowing it to be used in nuclear technologies. This process can be found in the operation of tritium-producing burnable absorber rods (TPBARs) in pressurized-water reactors. TPBARs utilize ceramic pellets of $^6LiAlO_2$, or other compounds containing ^6Li, which is then irradiated in a commercial power reactor with a large core by neutrons. As neutron is highly energetic, the combination of heat and radiation often damage all components of TPBARs as a result of exposure, diminishing their desired properties.[4, 5] Zirconium, however, is resistant damaged by neutron, due to having a low absorption cross-section, making it an ideal candidate for this extreme environment. The reaction of ^6Li and a neutron produces ^4He and T ($^6Li + n \rightarrow {}^4He + T$). The T then diffuses to the Zircaloy-4 getter, passing through a Ni coating, which reduces corrosion, and forms zirconium hydride (ZrT_x) for further extracting T_2.[6-9] In addition, T_2 also interacts with the oxide layer that forms on the zircaloy liner. The reactive metal like Zr usually interacts chemically with the water forming a layer of OH^- species on surfaces.

[a] National Energy Technology Laboratory, United States Department of Energy, Pittsburgh, PA 15236, USA
[b] Department of Chemistry, State University of New York at Buffalo, Buffalo, NY 14260-3000, USA
[c] NETL Support Contractor, 626 Cochran Mill Road, Pittsburgh, PA 15236, USA
[d] NETL Support Contractor, 1450 Queen Avenue SW, Albany, OR, 97321, USA
[e] Department of Chemistry, Hofstra University, Hempstead, NY 11549, USA
* To whom correspondence should be addressed. E-mail: Yuhua.duan@netl.doe.gov; Tel. 1-412-386-5771, Fax: 1-412-386-5990.

We have systematically investigated known T breeder compounds γ-$LiAlO_2$, Li_2TiO_3, and Li_2ZrO_3 in previous density functional theory (DFT) studies. The formation of T and its subsequent diffusion, as well as the impact of defects on these processes, has been thoroughly studied under operational conditions.[2, 3, 10-12] However, theoretical studies have yet to explore the surface interactions on Zr, while experiments are scarce due to the limited access to T and the resolution of experimental methods. In the TPBAR, liners reduce T_2O and T_2 released after the reduction is captured by getters. In presence of T_2O, oxidation of the liner's surfaces at low water partial pressure improves overall TPBAR performance for the T release.[13] There is still a lack of insight on the interaction of T_2O with the pure and oxidized liner surfaces that facilitates the nascent uptake of T during the oxidation. These facts represent gaps in our understanding, as TPBARs contain multiple layered components and possess several key interfaces between these materials, leading to the creation of surfaces between the Zr and other materials.[14, 15] To enhance our understanding of T behavior at all steps of the tritium production and capturing process, the Zr surface chemistry must be explored. Surfaces often possess unique properties when compared to the bulk materials, such as the ability to bind molecules and catalyze processes.[16] The process of binding molecules to the surface is known as adsorption. To date the adsorption of T on the T-getter Zircaloy-4, which contains 1.2-1.7 % tin to hinder corrosion, is not well understood.[17, 18] Rectifying this requires study of the basal (001) plane of Zr, as well as the prism (100) plane, the most energetically favored surfaces of Zr, and those most involved in slip deformations.[19, 20] Furthermore, as the Sn alloying of Zircaloy-4 results in Sn defects, the impact of Sn upon T adsorption should also be elucidated. Adsorption of T is the first step in the formation of ZrT_x, and crucial to the recovery of T. The process by which molecules or atoms move into the bulk of a material from the surface is known as absorption. This

process is the second step in the formation of ZrT_x, however the energy barriers and impact of defects on the absorption of T from the surface into the bulk are unknown. Previous studies posit that T diffusion in the bulk Zr is higher in the "*c*" crystallographic direction of the lattice than in the "*a*" direction due to the hexagonal space group of Zr. However, none of these studies have investigated the movement of T into the bulk along different Zr surfaces.[1]

Herein, we provide the results of DFT calculations of the T adsorption energies, and activation barriers for inter-site diffusion for surface-surface and surface-subsurface transfers on pure Zr and Sn-doped (less than 2%) Zr. We find that adsorption is more favorable on the basal Zr(001) surface. Sn impurities were found to lead to the repulsion of T atoms on the surface. Transport pathways from the surface into the bulk were found to be lower for Zr(001) than Zr(100). The presence of Sn impurities on absorption from the surface into the subsurface increased the energy barriers and hindered absorption.

Computational Details

All calculations were performed using the Vienna *Ab Initio* Simulation Package (VASP).[21, 22] The projector augmented wave (PAW) method was employed with the vdW-DF-optPBE density functional, which accounts for dispersion forces through a nonlocal correlation functional.[23, 24] It is important to include dispersion forces for computing adsorption energetics and structures at a metallic surface, making vdW-DF-optPBE an appropriate choice of functional in this study.[25-29] We utilized plane wave basis sets with a cutoff energy of 520 eV in conjunction with the PAW method. The T $1s^1$, Zr $5s^2 4d^2 5p^0$, and Sn $5s^2 5p^2$ electrons were treated explicitly in all calculations. The *k*-meshes were generated using the Γ-centered Monkhorst-Pack scheme, and the number of divisions along each reciprocal lattice vector was chosen such that the product of this number with the real lattice constant was 36 Å, corresponding to a 3 x 3 x 1 *k*-mesh.[30] The climbing-image nudged elastic band (cNEB) approach was used to calculate the transport barriers of T on the surfaces and in bulk Zr.[31-33] All initial and final images were optimized prior to the cNEB calculations. All transition states discovered were optimized and then used as the initial or final image for an additional cNEB calculation, ensuring the validity of the intermediate states. Only substitutional Sn defects were considered.[34] As in previous studies, the mass in the PAW POTCAR for ^{1}H was modified for the treatment of T.[12] This resulted in no changes to the electronic energy, as shown in the supporting information (Table S1). Calculations on Zr(001) utilized a slab of 100 atoms (a 5 x 5 x 2 supercell), corresponding to four layers of 25 atoms, while calculations on Zr(100) utilized a slab of 90 atoms (a 5 x 3 x 3 supercell), corresponding to six layers of 15 atoms. Zirconium surfaces were generated by performing geometry optimizations on experimentally refined structures.[35, 36] Each surface system was given a vacuum space of 20.0 Å along the z-axis to prevent interaction with the neighboring images. For the Zr(001) surface, the top two layers were allowed to fully relax during calculations with T, and for Zr(100) the top three layers were allowed to fully relax while the remaining layers were fixed to their bulk calculated lattice constants, which were within < 1% of experimental lattice constants.[35, 36] The convergence of the slab energies based off of the number of total and frozen layers are provided in the supporting information (Figures S1-S4 in section S2 and S3).

Results and Discussion

Determining the Binding Sites

To investigate where T adsorbs on the surface, the possible binding locations, visualized in Figure 1, on Zr(001) and Zr(100) and their respective energies were determined. The binding energy, E_{bind}, was calculated according to Equation 1 (Table 1), where E_{slab+T} represents the total energy of the system with T, E_{slab} represents the slab energy, and E_{T_2} represents the energy of the T_2 dimer.

$$E_{bind} = E_{slab+T} - E_{slab} - 0.5E_{T_2} \quad . \quad (1)$$

On Zr(001) both of the hollow, hexagonal close-packed (HCP) and face-centered cubic (FCC) are the most favorable binding sites, being nearly isoenergetic. Slightly higher in energy is the bridge site, however the binding interaction at this site is still favorable. The top site was found to have a positive binding energy, indicating that tritium adsorption to this site would not be favorable. The reason for this is that the Zr interacting with T rises out of the surface plane, which weakens its interactions with the neighboring Zr atoms, leading to a net unfavorable energy.

On Zr(100), T can bind at upper bridge, lower bridge, and step sites; while all Zr(100) sites have favorable binding energies, adsorption to the step site is preferred over either the upper or lower bridge sites. The step site can be interpreted as sitting in a hollow site with a plane corresponding to the Miller indices of (*1.5,0,-1*) in α-Zr. Both bridge sites for Zr(100) are close in energy, but in the upper bridge site the hydrogen interacts solely with the topmost termination layer, while in the lower bridge site the hydrogen interacts with both the uppermost and second termination layers (Figure 1). These additional interactions lead to an increased perturbation of Zr atoms, failing to offset the energy gained by additional Zr--H interactions, resulting in a higher energy.

Table 1. Calculated binding energies for T on Zr(001) and Zr(100) surface sites (Figure 1). A positive value of charge transfer indicates charge transfer from the surface to the T.

Surface	**(001)**	**(001)**	**(001)**	**(001)**	**(100)**	**(100)**	**(100)**
Binding Site	Top	Bridge	HCP	FCC	Upper Bridge	Lower Bridge	Step
E_{bind} (eV)	0.26	-0.74	-1.01	-0.99	-0.80	-0.77	-0.95
Charge Transfer (e^-)	0.52	0.62	0.64	0.64	0.59	0.66	0.63

For both the Zr (001) and Zr(100) surfaces, multiple binding sites with negative adsorption energies were discovered. If the barriers between these sites are sufficiently small, T could readily transfer between them. This is of particular importance

for transport from the surface to the subsurface, where the energy barrier to enter the subsurface could be affected by the binding site. Therefore, the energy barriers between the stable binding sites on the Zr surfaces were investigated for studies of the surface transport. For Zr(001), T movement from an FCC to HCP site was found to have an energy barrier of 0.27 eV (Figure 2). This FCC to HCP transfer moves the T through a bridge site, and the barrier to reach the bridge site is identical to the relative energy between the HCP and bridge sites of 0.27 eV. This suggests that T in the bridge site on the Zr(001) surface is a local maxima. Further supporting this is the observation that the T movement away from a bridge site to either a FCC or HCP site was found to be strictly downhill.

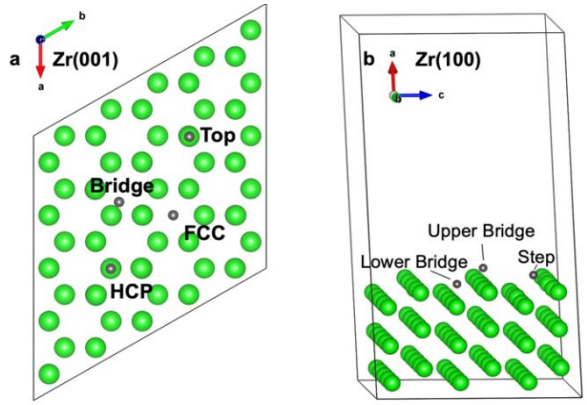

Figure 1. Binding sites for T on Zr(001) (a) and Zr(100) (b). T is represented by the small gray sphere, while Zr is colored green.

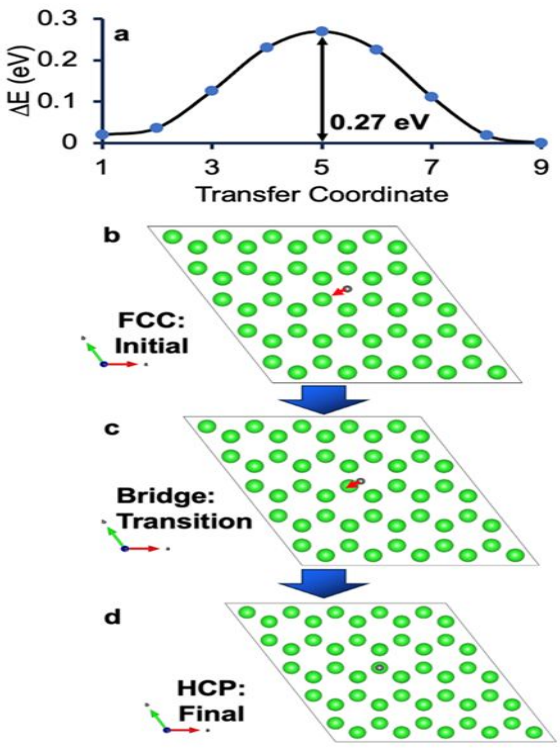

Figure 2. (a) Minimum energy pathway for the transfer of T on Zr(001) from (b) a FCC site through a (c) bridge site (approximate transition state) to (d) an HCP site.

For the Zr(100) surface, the transfer profile of T moving from an upper bridge site to a lower bridge site, passing through a step site was calculated (Figure 3). While both bridge sites are higher in energy than the step site, the barrier to reach the upper and lower bridge sites from the step site was calculated as being 0.15 eV and 0.45 eV, respectively. A transfer from a step site to a step site, passing through a lower bridge intermediate, was found to have an energy barrier of 0.45 eV (Figure 4), a barrier in agreement with the upper bridge to lower bridge transfer profile (Figure 3).

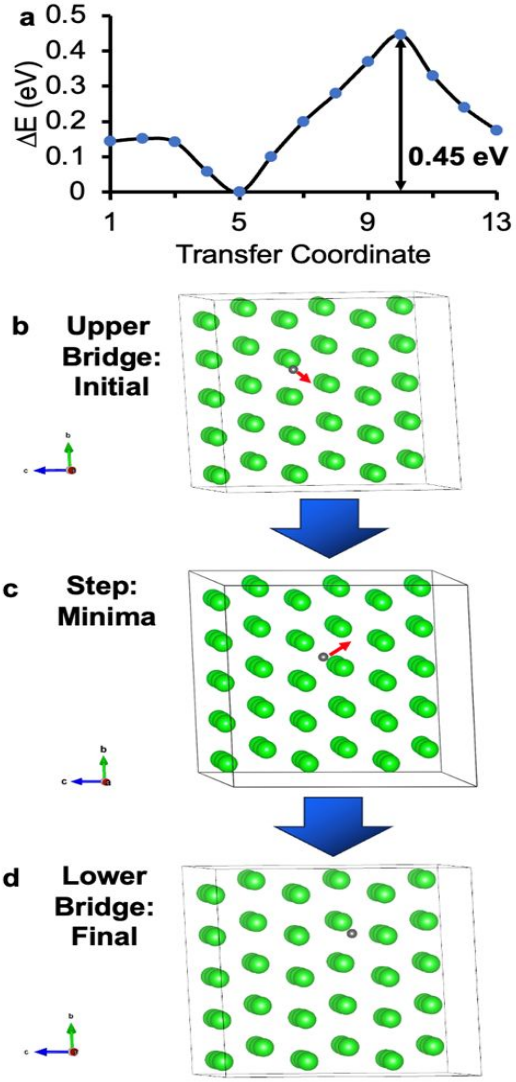

Figure 3. (a) Minimum energy pathway for the transfer of T on Zr(100) from (b) an upper bridge (transfer coordinate 1 in (a)) site through a (c) step site (transfer coordinate 5 in (a)) to (d) a lower bridge site (transfer coordinate 13 in (a)).

The binding of T_2 molecules to the Zr surfaces was also investigated, to determine if different binding sites would be favored. The dissociation of T_2 molecules on Zr surfaces is known to be a spontaneous process, prompting its investigation as a measure of computational accuracy. Geometry relaxations

were performed with T_2 molecules adsorbed in a side-on geometry to the possible binding sites. Side-on geometries were considered due to the known ability of transition metals, and their complexes, to bind H_2.[37] This process occurs due to H_2 donating σ electrons to a vacant d-orbital.[38] At least two different rotational orientations of the T_2 molecule were considered at each site to determine if the orientation had an effect on the binding energy. During the structural relaxation the dihydrogen molecules typically dissociated. To compare the simultaneous binding of the resulting two T atoms after dissociation from T_2, the binding energies (E_{bind}) were calculated according to the equation,

$$E_{bind} = E_{slab+2T} - E_{slab} - E_{T_2} \quad (2)$$

Table 2. Calculated binding energies for T_2 on Zr(001) and Zr(100) surface site. In some cases the optimized geometry resulted in a dissociation of the dihydrogen molecule, whereas in other cases the dimer remained intact. A single listed site means that dissociation of T_2 was not observed (*), while two listed sites indicate dissociation of T_2 into two separate T atoms (**).

Surface	**(001)***	**(001)***	**(001)****	**(001)****	**(100)***	**(100)****	**(100)****
Binding Site(s)	Top	FCC	Bridge, HCP	2x HCP	Top	2x Upper Bridge	2x Lower Bridge
E_{bind} (eV)	0.14	0.14	-1.71	-2.03	-0.06	-1.79	-1.10

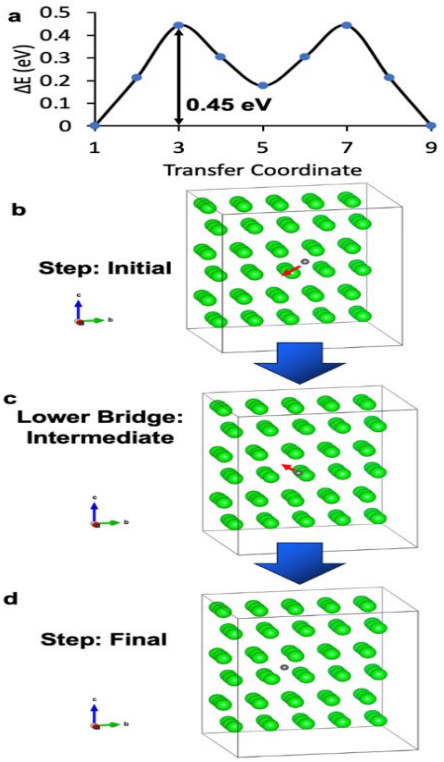

Figure 4. (a) Minimum energy pathway for the transfer of T on Zr(100) from (b) a step site (transfer coordinate 1 in (a)) passing through (c) a lower bridge intermediate (transfer coordinate 5 in (a)) to (d) a step site (transfer coordinate 9 in (a)).

Table 2 shows the calculated binding energies for T_2 on both Zr(001) and Zr(100). On Zr(001), T_2 generally dissociated when placed at HCP, FCC, and bridge sites, but remained as T_2 when placed on a top site. Calculations indicated that this process is sensitive to the tilt of the T_2 atom; when a tilt of 30˚ was applied (lifting one of the T atoms up from the surface plane), a T_2 molecule on an FCC site failed to dissociate. On Zr(100), T_2 dissociated when placed at non-top sites to form two T's on bridging sites. The binding energies obtained from the T_2 dissociation studies are similar to those obtained from the T binding studies, taking the binding site and number of T's bound into consideration. It is worth noting that the calculations performed take place with minimal T coverage, and neglect temperature. In real systems, we expect both a larger coverage and thermal effects, which may have an impact on the binding energies or lead to T---T interactions on the surface.

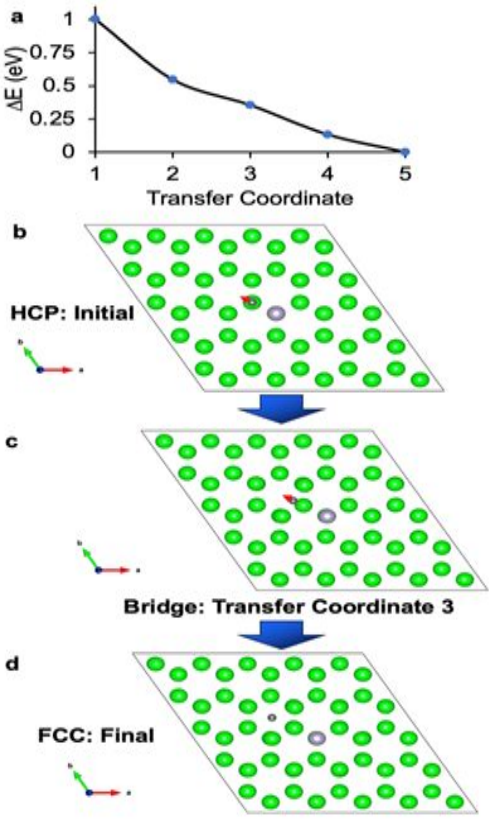

Figure 5. (a) Surface repulsion of T by Sn from (b) an HCP site (transfer coordinate 1) through (c) a bridge site to (d) an FCC site (transfer coordinate 5) on Zr(001).

Sn Defects on the Zr Surface

Zircaloy-4 alloy consists almost entirely of Zr but contains 1.2-1.7% Sn.[39] Studies suggest that it is adequate to model Zircaloy-4 using pure Zr, however the effect of impurities has so far been omitted.[40] However, with large systems, such as our Zr(001) and (100) surfaces, which contain 100 and 90 atoms, respectively, the impurities can be explicitly modeled. By introducing a substitutional defect, where one Zr atom is replaced with a Sn atom, we obtain Sn percentages of 1.00% and 1.11%, respectively, in good accordance with the composition of Zircaloy-4.[39] Sn defects were introduced to the Zr surfaces, at selected surface or subsurface sites, to investigate the impact of Sn on T binding and absorption energy.

To better understand the effect of Sn on the interaction of T with the surface, geometry optimizations were performed for each binding site on the Zr(001) and Zr(100) surface with a Sn substitutional defect in a first nearest neighbor (1NN) position to the T. For the Zr(001) surface, when T was relaxed in the presence of a 1NN Sn, a repulsive effect was observed. This process is illustrated in Figure 5, which shows the T steadily moving further away from the Sn in a strictly downhill process. Both FCC and HCP T's, when their 1NN was Sn, would migrate from their site to the next nearest hollow site, out of interaction range with Sn. In contrast, T would relax to a top site (on a Sn atom) and a bridge site (adjacent to a Sn atom), however neither of these sites were calculated to have stable binding energies. On the Zr(001) surface, we can compare the binding energies of -0.74 eV (bridge site, pure Zr in Table 1) to 0.24 eV (bridge site, Sn defect), and the value of 0.26 eV (top site, pure Zr in Table 1) to 1.01 eV (top site, Sn defect) to see significant increases in energy caused by the presence of an Sn atom. On the Zr(100) surface, similar effects were observed with regards to the presence of Sn on the T binding, with numerical values provided in Table 3. When T occupies an upper bridge site in the presence of Sn, the binding becomes unfavorable. Furthermore, when T is relaxed in the presence of Sn in a lower bridge site, the T migrates to a step site to minimize Sn interactions. The reverse of this process occurs when T is relaxed in the presence of Sn on a step site. The presence of Sn alone causes T to transfer sites on the surface, and no sites where T and Sn interact favor binding, indicating strong repulsive behavior between Sn and T. These examples of the repulsive effect of Sn on T binding and diffusion are in agreement with published findings.[15, 40, 41]

The effect of Sn defects on T_2 was also investigated to determine the impact on binding and dissociation. Similar to that of T interacting with Sn on the surface, it was found that Sn was repulsive to T_2 with the exception of the FCC site on Zr (001), as seen for the investigated sites in Table 4. In the case of the FCC site on Zr (001), while one of the T atoms did bind in an FCC site on Sn, the total binding energy of the system (-1.04 eV) becomes less favourable by 0.96 eV compared to the binding energy of the same sites on the pure Zr system (HCP: -1.01 eV, FCC: -0.99 eV, total: -2.00 eV). This further supports the instability of T on the Sn sites. However, one interesting outcome is an increased stability of T_2 after being repulsed by Sn, as compared to the dissociation of T_2 observed for the majority of sites on the pure Zr surfaces (see Table 2).

Table 3. Results of calculations where the position of T was relaxed in the presence of Sn on Zr surfaces. Binding energies are omitted for systems where the Sn repulsed the T to a different binding site.

Surface	**(001)**	**(001)**	**(001)**	**(001)**	**(100)**	**(100)**	**(100)**
Initial Site	Top	Bridge	HCP	FCC	Upper Bridge	Lower Bridge	Step
Final Site	Top	Bridge	FCC	HCP	Upper Bridge	Step	Lower Bridge
Final Site on Sn?	Yes	Yes	No	No	Yes	No	No
E_{bind} (eV)	1.01	0.24	--	--	0.22	--	--

Table 4. Results of calculations where the position of T_2 was relaxed in the presence of Sn on Zr surfaces, with Sn as the first nearest neighbor. Binding energies are omitted for systems where the Sn repulsed the T_2 to a different binding site.

Surface	**(001)**	**(001)**	**(001)**	**(001)**	**(001)**	**(100)**	**(100)**	**(100)**
Initial Site	Top	Bridge (T_2 parallel)	Bridge (T_2 perpendicular)	HCP	FCC	Upper Bridge	Lower Bridge	Step
Final Site	Top	Top	HCP FCC	Top	HCP (off Sn) FCC (on Sn)	Top	Upper Bridge Upper Bridge	Lower Bridge
Dissociated?	No	No	Yes	No	Yes	No	Yes	No
Final Site(s) on Sn?	No	No	No	No	FCC	No	No	No
E_{bind} (eV)	--	--	--	--	-1.04	--	--	--

Surface to Subsurface Transfer

While the diffusion of T through zirconium bulk has been previously studied, the effect of surfaces on this process is so far unexplored.[15, 41] Several possible pathways exist for the transfer of T from the surface to the bulk of Zr(001); herein we

considered the transfer from an FCC site on the surface to an octahedral site in the bulk. The barrier for this process was computed to be 0.70 eV, and shortly after overcoming this barrier along the pathway, the T encounters a local minimum (Figure 6, coordinate 5). The highly irradiated environment to which the TPBARs are subject provides a substantial amount of energy, which makes it plausible that a barrier of this height could be readily overcome. Additionally, this surface to bulk transfer process is supported by the latent pressure applied to the getter from T gas produced by the irradiation process, leading to T permeating the Zr.[42] From this local minimum, an energy barrier of 0.53 eV must be overcome to reach the bulk octahedral site (coordinate 9), contrasted by an energy barrier of 0.10 eV to return to the surface (coordinate 1). The reverse transfer process, from the bulk octahedral site (coordinate 9) to the subsurface octahedral site (coordinate 5) has an energy barrier of 0.61 eV, which is in agreement with results obtained in previous calculations on the octahedral-octahedral diffusion of T in bulk Zr.[3, 15, 41]

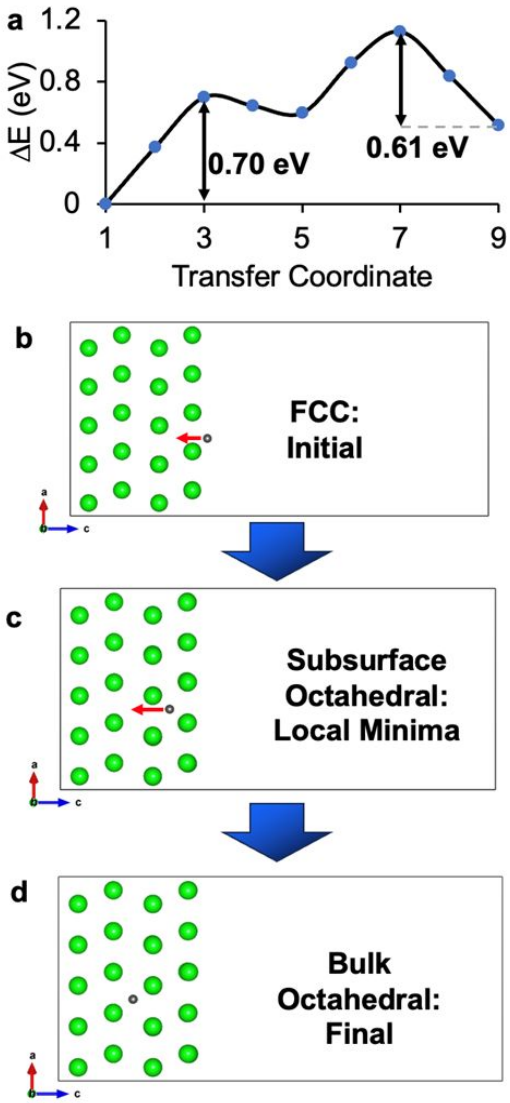

Figure 6. (a) Minimum energy pathway for the transfer of T on Zr(001) from (b) a FCC site on the surface (transfer coordinate 1) to (c) a subsurface octahedral site (transfer coordinate 5) and then to (d) a bulk octahedral site (transfer coordinate 9).

There are several possible paths through which T could diffuse into Zr(100). In this study, paths starting at a step site and then moving into the subsurface were considered as the most promising candidates, due to the step site possessing the most stable binding energy on the Zr(100) surface. An overview of one such proposed process is shown below in Figure 7. The energy rises steeply during the course of the transfer process, having to overcome an energy penalty of 1.11 eV to reach the tetrahedral site. Additionally, the reverse transfer barriers, from transfer coordinates 6 to 5 and 11 to 10, are < 20 meV, which would correspond to enough energy being present for the reverse transfer at room temperature. The substantial increase in energy during this transfer is largely due to the Zr atom above T moving in the *a*-axis direction, away from the bulk, to accommodate T moving into the bulk. Geometries where T had a direct path to the surface, without being physically blocked by a Zr, resulted in the T returning to the surface during the optimization process, as opposed to remaining in the subsurface. However, geometries where the T was blocked by a Zr atom showed significant distortion coupled with a substantial increase in energy. It is likely that other pathways exist for this process, but alternative paths have not yet been considered herein.

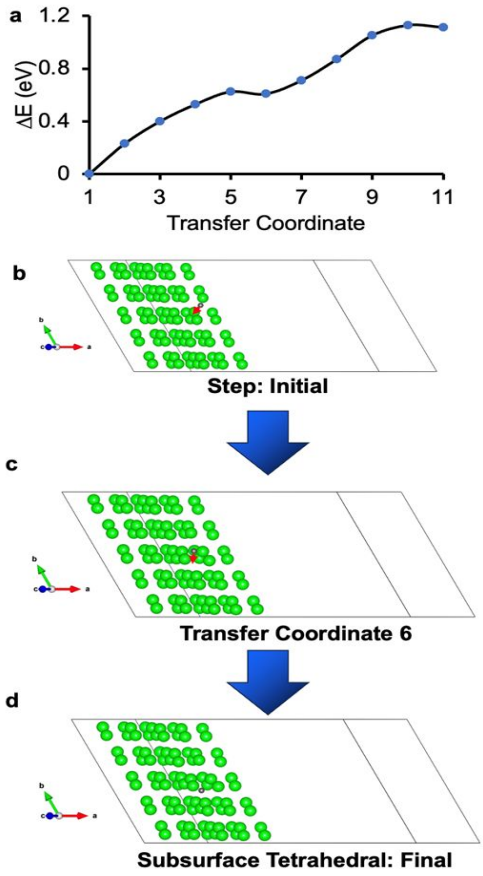

Figure 7. (a) Energy profile for the transfer of ^{3}H on Zr(100) from (b) a step site on the surface (transfer coordinate 1) through (c) a position just below the surface to (d) a subsurface tetrahedral site (transfer coordinate 6).

Surface to Subsurface Transfer with Impurities

The effect of Sn impurities on the T absorption process was investigated for Zr(001), as the surface to subsurface to bulk transfer of T was found to be more favorable for Zr(001) than for Zr(100). When Sn is on the surface, the surface to subsurface transfer energy barrier to an octahedral site was calculated to be 0.77 eV as shown in Figure 8, an increase of 0.07 eV from the same process on a pristine surface. Interestingly, the approximate transition state for this process appears not at the midpoint of the distance travelled by the T, but instead somewhat afterwards, due to the energy penalty imposed by the Sn. The energy barrier for the reverse transfer is calculated to be 0.09 eV, within 0.01 eV of the reverse transfer process for the pristine surface. While these similar energies for the pristine and impure systems speak to the similar transfer processes occurring, it must be noted that this process is significantly less likely to occur in the presence of Sn, as the T will spontaneously transfer on the surface to a hollow site without Sn interactions, making this pathway more difficult to access.

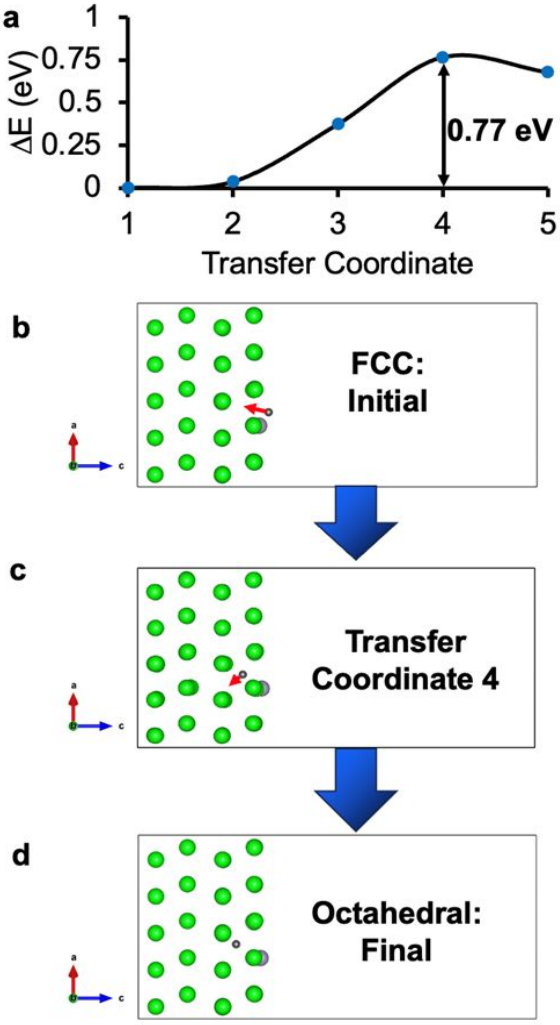

Figure 8. (a) Minimum energy pathway for the transfer of T on Zr(001) from (b) a FCC Sn site on the surface (transfer coordinate 1) through the (c) surface layer to (d) a subsurface octahedral site (transfer coordinate 5).

For the transfer process when the Sn is located in the subsurface, the T atom must overcome the repulsive effect of Sn to reach the octahedral site. This results in a significantly higher energy barrier, seen in Figure 9, of 1.47 eV, almost double the energy barrier for the same transfer with Sn on the surface. However, if this barrier is overcome, we observe a significant barrier for the reverse transfer at 0.83 eV. This barrier for the reverse reaction is the largest calculated for the reverse transfer processes in this study, indicating that the Sn can assist in energetically "trapping" T within the bulk. Furthermore, this indicates that if T is in this site, transferring to a site further from the Sn, but not towards the surface, is energetically favored.[3, 15, 41] When we measure the distance that T is from the surface atom layer for the system with Sn on the surface (Figure 8), we see that the T sits 1.39 Å below the

surface. However, for the system with Sn in the subsurface (Figure 9), the T sits 0.92 Å below the surface. Each of these distances correspond to the T being repulsed by Sn, either towards the bulk or towards the surface, respectively (cf. Figures 8d and 9d).

Diffusion coefficient

The likelihood of a T to transfer between sites, corresponding to the diffusion coefficient, cannot be determined solely based on the energy barriers, as the effect of temperature is excluded in the calculations of the approximate barriers. In an energetic environment, such as the one found during the irradiation process of TPBARs, radiation and temperature provide additional energy to overcome sizable transfer barriers. The likelihood of a T transfer to occur, and the diffusivity of T on the surface can be modeled using the Einstein–Smoluchowski relation.[43] The diffusion coefficient, *D*, is expressed as

$$D = \frac{a^2}{c\tau} \quad (3)$$

where *a* is the average distance between jumps, τ is the average time between jumps, and *c* is a value corresponding to the translational degrees of freedom, being 2 in 1-D, 4 in 2-D, and 6 (our selected value) in 3-D. By expressing *D* in terms of the transfer barrier, E_T, and vacancy formation energy, Q_V, we obtain equation 4, where R_0 is the attempt frequency and *z* the coordination number, being 3 for the surface hollow sites and 6 for the bulk octahedral sites:

$$D \approx \frac{a^2}{6} R_0 z e^{-(E_T+Q_V)/k_B T} \quad . \quad (4)$$

The attempt frequency R_0 is the vibrational frequency of the adsorbed or absorbed molecule, herein T, and is generally of the order of 10^{13} s^{-1}. The probability of a transfer can be obtained from the time between transfers, τ, estimated through equation 5:

$$\tau \approx \frac{1}{R_0 z} e^{(E_T+Q_V)/k_B T} \quad . \quad (5)$$

Both on the surface of Zr and within the bulk, vacancies are available for T to transfer to, ergo these vacancies do not require energy to form, yielding $Q_V = 0$. This assumption is easily justified on the surface, as the number of available hollow sites far exceed the number of T atoms. For the bulk Zr, we can consider a system where there are *Nv* vacancies distributed throughout the crystal. The increase in entropy (∂S) added per vacancy in the crystal ($\partial S_{mix}/\partial Nv$) caused by the creation of vacancies after mixing is proportional to −ln(*Nv*/(1 − *Nv*)). As *Nv* approaches 0, the change in entropy approaches infinity, $\partial S_{mix}/\partial Nv \rightarrow \infty$, indicating a system in a state of non-equilibrium. Therefore, the thermodynamic equilibrium Zr crystal system must have a non-zero concentration of vacancies. While this assumption can be broadly extrapolated to other systems, this assumption is supported even more so for systems being subject to intense irradiation where neutron bombardment and knock-on atoms serve to further increase the population of vacancies.

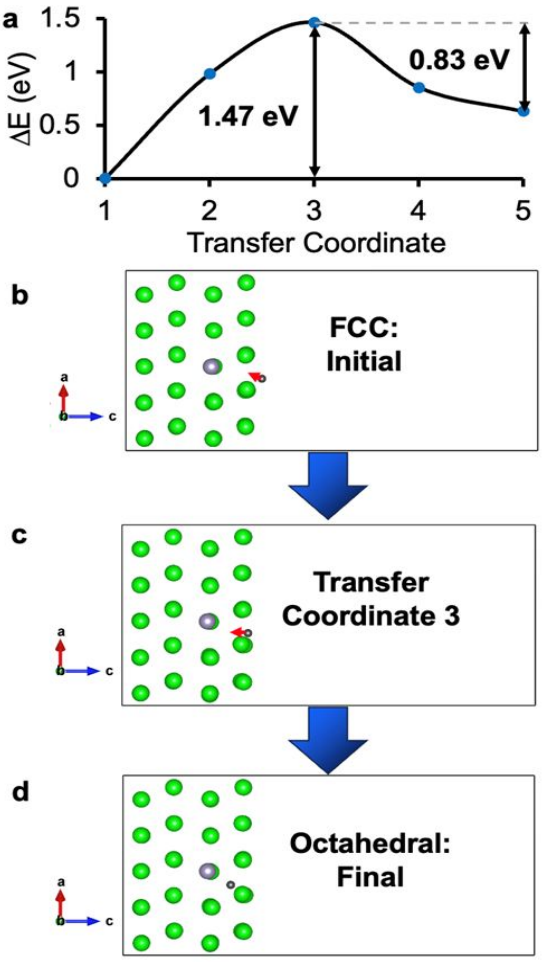

Figure 9. (a) Minimum energy pathway for the transfer of T on Zr(001) from (b) a FCC site on the surface (transfer coordinate 1) through (c) the surface layer to (d) a subsurface Sn octahedral site (transfer coordinate 5).

The diffusion coefficients for T transfer along the Zr surface were calculated at several temperatures, shown in Figure 10, corresponding to TPBAR operating conditions. For the Zr(001) surface, *D* was calculated for transfers from HCP-FCC sites. The diffusion coefficient was found to be 9.53 x 10^{-10} m^2s^{-1} at 600 K, decreasing to 5.14 x 10^{-12} m^2s^{-1} at 300 K. For the Zr(100) surface, calculated values of 1.30 x 10^{-10} m^2s^{-1} and 3.17 x 10^{-14} m^2s^{-1} were found for the diffusion coefficient with regards to the step-step site transfer at 600 and 300 K, respectively. The calculated diffusion coefficients suggest that T transfer is more facile on Zr(001) than Zr(100), corresponding to the respective calculated energy barriers to T transfer on the surfaces. Even more facile than the Zr(001) hollow site T transfer is T transfer in the bulk, with the minimum bulk transfer barrier being 0.23 eV, corresponding to a tetrahedral-tetrahedral transfer and a diffusion coefficient of 2.49 x 10^{-8} m^2s^{-1} at 600 K.[37] This suggests that T transfer, while still occurring on the surface, is two orders of magnitude more mobile in the bulk of Zr.

The diffusion coefficients for T transfer from the surface to the subsurface were also calculated with and without the presence

of Sn impurities on the Zr(001) surface. T transfer from the surface to the subsurface in a pristine Zr crystal was found to have a diffusion coefficient of 5.14 x 10^{-13} m^2s^{-1} at 600 K and 6.78 x 10^{-19} m^2s^{-1} at 300 K. This rate is smaller than the surface-surface transfer, but still occurs, albeit with a value of *D* lessened by 4 orders of magnitude. When Sn is on the surface, this rate is found to drop to 1.58 x 10^{-13} m^2s^{-1} at 600 K, and diminishes to 5.39 x 10^{-20} m^2s^{-1} at 300 K. The presence of Sn alone causes a three-fold drop in diffusivity at 600 K. When compared to a subsurface Sn impurity, the diffusion coefficient drops precipitously to 1.45 x 10^{-19} m^2s^{-1}, and then lower again to 6.54 x 10^{-32} m^2s^{-1} at 600 and 300 K, respectively. The repulsive nature of Sn is clearly demonstrated through the significantly reduced diffusivities compared to the defect-free system, listed in Table 5.

The diffusion coefficients given previously apply for the absorption processes of T on Zr. While absorption is the process of interest during irradiation, the subsurface to surface transfer process (StSTP) is relevant for the extraction and recovery of the stored T in the Zr. The StSTP can be viewed as the reverse transfer of the absorbative transfer. Thus, the transfer barriers for the StSTP can be obtained from the adsorption process, by using the reverse barrier, and corresponding diffusion coefficients can be calculated. Calculated diffusion coefficients for the StSTP at different temperatures are shown in Figure 11. The subsurface-surface transfer process on the pristine surface has a barrier of 0.10 eV (Figure 6a), markedly similar to the subsurface-surface Sn transfer process with a barrier of 0.09 eV (Figure 8a), resulting in diffusion coefficients of 5.64 x 10^{-8} m^2s^{-1} and 8.16 x 10^{-8} m^2s^{-1} at 600 K, respectively. These diffusion coefficients are much larger than that for the transfer of T from a subsurface site with Sn to the pure surface, which has a value of 3.46 x 10^{-14} m^2s^{-1} at 600 K. These StSTPs produce larger diffusion coefficients than the absorptive processes, due to having smaller energy barriers. Furthermore, the diffusion coefficients are larger for the StSTP transfers, for pure Zr and the surface Sn impurity system, than for transfers occurring in the bulk system. It is worth noting that the presence of Sn on the surface appears to do little to hamper the StSTP, and in fact enhances it slightly. In contrast to this, when Sn is present as a subsurface impurity, the diffusion coefficient greatly diminishes. For the subsurface Sn – surface T transfer, the absorption transfer barrier is greater than the barrier for the StSTP, in line with the other calculated StSTPs. This subsurface Sn – surface T transfer, with an energy barrier of 0.83 eV (Figure 9a), must overcome a larger energy than the bulk tetrahedral – tetrahedral transfer with one Sn impurity (0.60 eV, Figure 6 in ref. 37), indicating that the subsurface to surface transfer is less favorable than transferring to a different site in the bulk in the presence of Sn.[41] For all transfers investigated, the StSTP was found to be more energetically favorable and have a larger diffusion coefficient than the corresponding absorption process.

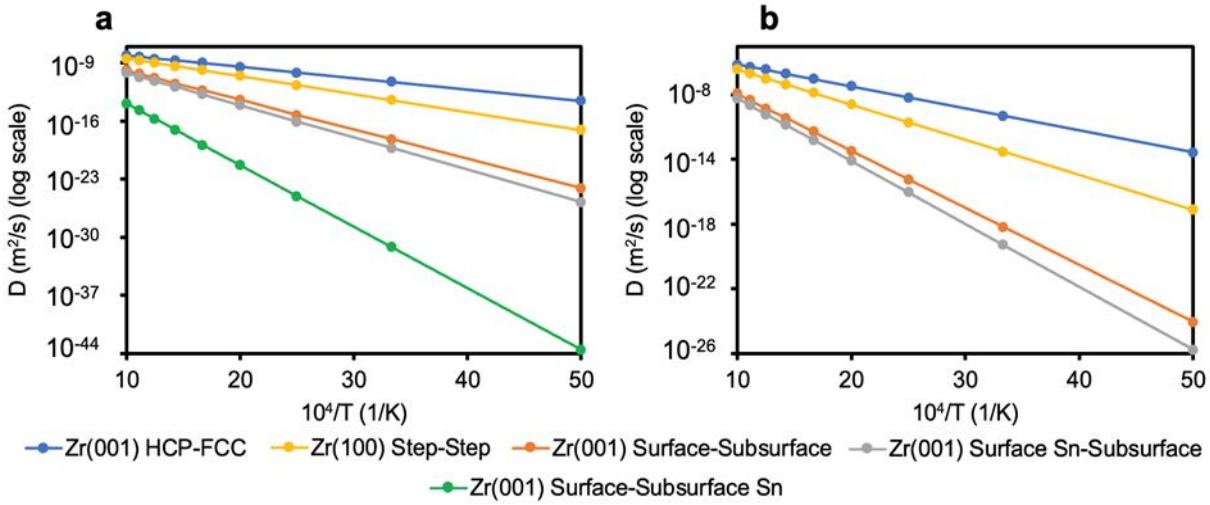

Figure 10. Calculated diffusion coefficients for the surface-surface and surface-subsurface transfer processes on Zr in the pristine material and with Sn impurities at temperatures ranging from 200-1000 K. The transfer profiles for Zr(001) HCP-FCC, Zr(100) Step-Step, Zr(001) Surface-Subsurface, Zr(001) Surface Sn-Subsurface, and Zr(001) Surface-Subsurface Sn are given in Figure 2, Figure 4, Figure 6, Figure 8, and Figure 9, respectively. (a) Includes the Zr(001) surface to subsurface transfer with a Sn impurity in the subsurface. This transfer process was found to have the highest energy barrier, and as such would be less likely than the other transfer processes, leading to (b), where the least likely transfer is omitted.

Table 5. Calculated diffusion coefficients for T transfer processes on pure and Sn defective Zr at 600 K, as well as in bulk Zr at 600 K. Diffusion coefficients for T transfer in bulk Zr are from ref. 37.

Transfer	Transfer Barrier (eV)	Diffusion Coefficient at 600 K (m^2s^{-1})
Zr(001) HCP - FCC	0.27	9.53 x 10^{-10}

Zr(001) Surface - Subsurface	0.70	5.14×10^{-13}
Zr(001) Surface with Sn impurity – Subsurface	0.77	1.58×10^{-13}
Zr(001) Surface – Subsurface with Sn impurity	1.47	1.45×10^{-19}
Zr(100) Step – Step	0.43	1.30×10^{-10}
Bulk Zr Tetrahedral - Tetrahedral	0.23	2.49×10^{-8}
Bulk Zr Tetrahedral - Tetrahedral with one Sn impurity (0.67% concentration)	0.60	4.18×10^{-12}

It is worth noting that the accuracy of the transfer barriers and diffusion coefficients are subject to the limitations arising from DFT. Exact methods to treat the exchange-correlation energy do not exist. T is known to participate in quantum tunneling, which can lead to an underestimation of *D* by up to 10%.[40, 44] In our DFT calculations, which were performed at 0 K for classical nuclei, the entropic contribution term is neglected for *D*. At finite temperature, the deviation between the calculated and observed *D* could increase with temperature, due to the effects of entropy and vacancy concentration. Fortuitously, previous DFT studies have found that for the FCC Al system, the enthalpy and entropy terms affected by temperature provide an error canceling effect.[32] This leads to a negligible effect of temperature on the calculated diffusion coefficients, which were found to be in good experimental agreement.[45] Additionally, this study neglected the effect of the presence of multiple T atoms or Sn defects on the surface and/or subsurface, which could affect transfer barriers due to additional interactions. Lastly, the StSTP requires that there be an available binding site for T on the Zr surface. The Zr surface, with an average T binding energy of 1 eV at hollow sites, was calculated to be a more energetically favored site than the subsurface. For the StSTP to occur, the surface T must first desorb, overcoming the binding energy to escape the Zr. Therefore, this indicates that the calculated StSTP diffusion rate may be limited by the T desorption rate, as the T serves as a cap, hindering subsurface and bulk T from reaching the surface and desorbing. Despite this, the results presented provide initial estimates for diffusion coefficients and may be used as guideposts for future studies.

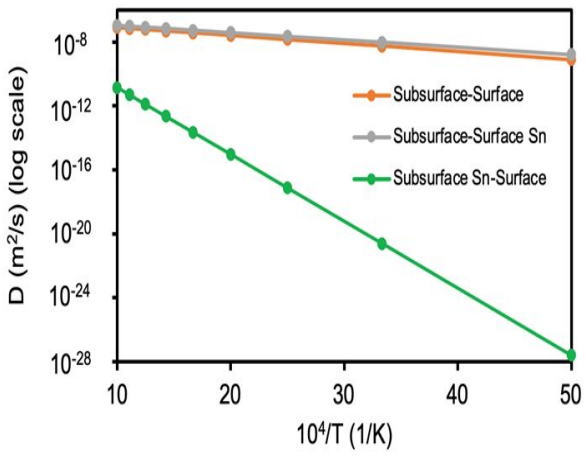

Figure 11. Calculated diffusion coefficients for the subsurface to surface transfer processes of T in Zr(001) for both the pristine system and ones with Sn substitutional defects.

Conclusions

Better understanding of the chemical properties of zirconium are necessary to reach ultimate performance capabilities in tritium production with TPBARs. To this end we have assessed the surface chemistry of Zr interacting with T holistically based upon dispersion-including density functional theory calculations. The relative energies of T binding sites on Zr(001), favoring hollow sites, and Zr(100), favoring a step site, were determined. The surface-surface transfer barriers for T on these surfaces were calculated. Sn substitutional impurities were shown to strongly repel the adsorbed T. Possible paths for surface to bulk diffusion are proposed, with diffusion being more facile on the Zr(001) surface. Our results reproduce both the spontaneous dissociation of T_2 on Zr and previously calculated minimum energy pathways for the transfer of T in bulk Zr. Surface to subsurface transfer of T with Sn on the surface produces a similar minimum energy pathway to that of the pristine surface. The counterpart of this, the transfer from a pristine surface to a Sn impure subsurface, produces significant energy barriers for both the forward and reverse reactions, indicating subsurface Sn will hinder the release of T. A surface-subsurface diffusion coefficient of 5.64×10^{-8} m^2s^{-1} at 600 K was calculated, with Sn impurities determined to reduce this diffusion coefficient by up to 9 orders of magnitude. Diffusion coefficients for the reverse absorption of T were also calculated and found to be 5.14×10^{-13} m^2s^{-1} at 600 K for pure Zr. This work sheds light on T adsorption and absorption mechanics in Zircaloy, motivating future research for Zr-based T getters.

Author contributions

Conceptualization, Y.D., H.P., and D.T.; methodology, M.R.; software, Y.D.; validation, M.R.; formal analysis, M.R.; investigation, M.R.; resources, Y.D., E.Z., and D. M.; data curation, M.R.; writing—original draft preparation, M.R.; writing—review and editing, H.P., D.S., M.P. E. Z., and Y.D.; visualization, M.R.; supervision, Y.D. H.P., and E.Z.; project administration, Y.D; funding acquisition, Y.D. All authors have read and agreed to the published version of the manuscript.

Conflicts of interest

There are no conflicts to declare.

Data availability

The raw/processed data required to reproduce these findings cannot be shared at this time due to technical or time limitations but may be obtained by contacting corresponding author. This research used VASP software which can be found at www.vasp.at. The version of VASP employed for this study is 5.4.4.

Acknowledgements

This research was supported in part by an appointment with the AMMTO Summer Internships program sponsored by the U.S. Department of Energy (DOE), EERE Advanced Materials and Manufacturing Technologies Office (AMMTO). This program is administered by the Oak Ridge Institute for Science and Education (ORISE) for DOE. ORISE is managed by ORAU. All opinions expressed in this paper are the author's and do not necessarily reflect the policies and views of DOE, ORAU, or ORISE. Calculations were performed using JOULE 2.0 at the NETL and at the Center for Computational Research at SUNY Buffalo (https://hdl.handle.net/10477/79221). Partial funding for this research was provided by the U.S. Department of Energy (DOE), National Nuclear Security Administration (NNSA), through the Chicago-DOE Alliance Center (CDAC) under Cooperative Agreement DE-NA0003975 (E.Z. and M.R). This research was also supported in part by the NNSA DOE through the Tritium Science Research Supporting the Tritium Modernization Program.

Disclaimer

Supporting Information

The Supporting Information is available free of charge on the publication website, https://pubs.acs.org/. It includes the energy of ^{1}H and T systems, surface energy convergence, the energies as a function of frozen layers, Bader charges, density of states, and structural coordinates.

Notes and references

1. J. J. Kearns, *J Nucl Mater*, 1972, **43**, 330-338.
2. H. Paudel, Y. L. Lee, D. Senor and Y. Duan, *J Phys Chem C*, 2018, **122**, 9755-9765
3. C. M. Andolina, W. A. Saidi, H. P. Paudel, D. J. Senor and Y. Duan, *Comp Mater Sci*, 2022, **209**, 111384.
4. A. T. Motta, A. Couet and R. J. Comstock, *Annual Review of Materials Research*, 2015, **45**, 311-343.
5. A. S. Zaimovskii, *Soviet Atomic Energy*, 1978, **45**, 1165-1168.
6. J.-S. Kim, S.-D. Kim and J. Yoon, *J Nucl Mater*, 2016, **482**, 88-92.
7. A. T. Motta and L.-Q. Chen, *JOM*, 2012, **64**, 1403-1408.
8. G. Dey, K., S. Banerjee and P. Mukhopadhyay, *J. Phys. Colloques*, 1982, **43**, C4-327-C324-332.
9. L. Thuinet and R. Besson, *Intermetallics*, 2012, **20**, 24-32.
10. H. Paudel, Y.-L. Lee, J. Holber, D. C. Sorescu and Y. Duan, *Fundamental Studies of Tritium Solubility and Diffusivity in LiAlO2 and Lithium Zirconates Pellets Used in TPBAR*, DOE-National Energy Technology Laboratory, DOE/NETL-PUB-21464, doi: 10.2172/1463897, 2017.
11. Y. Lee, S. D. Barthel, P. Dłotko, S. M. Moosavi, K. Hess and B. Smit, *Journal of Chemical Theory and Computation*, 2018, **14**, 4427-4437.
12. Y. Duan, D. C. Sorescu, W. L. Jiang and D. J. Senor, *J Nucl Mater*, 2020, **530**, 152963.
13. W. Jiang, S. R. Spurgeon, B. E. Matthews, A. K. Battu, S. China, T. Varga, A. Devaraj, E. J. Kautz, M. A. Marcus, D. D. Reilly and W. G. Luscher, *Nuclear Materials and Energy*, 2020, **25**, 100797.
14. T. Jia, D. J. Senor and Y. Duan, *Applied Surface Science Advances*, 2021, **5**, 100114.
15. T. Jia, H. P. Paudel, D. J. Senor and Y. Duan, *Comp Mater Sci*, 2022, **203**, 111158.
16. G. A. Somorjai and Y. Li, *Introduction to surface chemistry and catalysis*, John Wiley & Sons, 2010.
17. P. Rudling and B. Kammenzind, *Zirconium in the Nuclear Industry: Fourteenth International Symposium*, ASTM International, 2005.
18. H. G. Rickover, L. D. Geiger and B. Lustman, *History of the development of zirconium alloys for use in nuclear reactors*, Energy Research and Development Administration, Washington, D.C. (USA). Div. of Naval Reactors, United States, 1975.
19. H. G. Kim, T. H. Kim and Y. H. Jeong, *J Nucl Mater*, 2002, **306**, 44-53.
20. J. Gong, T. B. Britton, M. A. Cuddihy, F. P. Dunne and A. J. Wilkinson, *Acta Materialia*, 2015, **96**, 249-257.
21. G. Kresse and J. Furthmuller, *Phys. Rev. B*, 1996, **54**, 11169-11186.
22. G. Kresse and D. Joubert, *Phys Rev B*, 1999, **59**, 1758-1775.
23. J. P. Perdew, K. Burke and M. Ernzerhof, *Physical Review Letters*, 1996, **77**, 3865-3868.
24. P. E. Blöchl, *Phys Rev B*, 1994, **50**, 17953-17979.
25. J. Klimeš, D. R. Bowler and A. Michaelides, *J Phys Condens Matter*, 2010, **22**, 022201.
26. J. Klimeš, D. R. Bowler and A. Michaelides, *Phys Rev B*, 2011, **83**, 195131.
27. M. Dion, H. Rydberg, E. Schröder, D. C. Langreth and B. I. Lundqvist, *Physical Review Letters*, 2004, **92**, 246401.
28. T. Thonhauser, V. R. Cooper, S. Li, A. Puzder, P. Hyldgaard and D. C. Langreth, *Phys Rev B*, 2007, **76**, 125112.
29. G. Román-Pérez and J. M. Soler, *Physical Review Letters*, 2009, **103**, 096102.
30. H. J. Monkhorst and J. D. Pack, *Phys. Rev. B*, 1976, **13**, 5188-5192.
31. G. Henkelman, B. P. Uberuaga and H. Jónsson, *The Journal of Chemical Physics*, 2000, **113**, 9901-9904.
32. G. Henkelman and H. Jónsson, *The Journal of Chemical Physics*, 2000, **113**, 9978-9985.
33. D. N. Tafen, H. P. Paudel, D. J. Senor, A. M. Casella and Y. Duan, *Physical Chemistry Chemical Physics*, 2025, **27**, 481-489.
34. C. Freysoldt, J. Neugebauer and C. G. Van de Walle, *Physical Review Letters*, 2009, **102**, 016402.
35. J. Goldak, L. T. Lloyd and C. S. Barrett, *Phys Rev*, 1966, **144**, 478-484.
36. J. Zheng, H. Zhang, X. Zhou, J. Liang, L. Sheng and S. Peng, *Adv. Cond. Matter. Phys.*, 2014, **2014**, 929750.
37. G. J. Kubas, *Chemical Reviews*, 2007, **107**, 4152-4205.
38. J. Y. Saillard and R. Hoffmann, *J Am Chem Soc*, 1984, **106**, 2006-2026.
39. G. Sabol, P. Rudling and B. Kammenzind, in *Zirconium in the Nuclear Industry: Fourteenth International Symposium*, ASTM International, 2005, vol. STP1467-EB, p. doi: 10.1520/stp37500s.
40. Y. Zhang, C. Jiang and X. Bai, *Scientific Reports*, 2017, **7**, 41033.
41. H. P. Paudel, T. Jia, W. A. Saidi, D. J. Senor, A. M. Casella and Y. Duan, *The Journal of Physical Chemistry C*, 2023, **127**, 12435-12443.
42. D. F. Cowgill, *Tritium Pressure Enhancement on the TPBAR Cladding by Physical Processes at the Getter*, United States, 2020.
43. P. Shewmon, *Diffusion in Solids*, Springer International, Switzerland, 2016.
44. D. S. Sholl, *J. Alloys Compd.*, 2007, **446-447**, 462-468.
45. M. Mantina, Y. Wang, R. Arroyave, L. Q. Chen, Z. K. Liu and C. Wolverton, *Physical Review Letters*, 2008, **100**, 215901.

Data for this article, including information on TPBARs and tritium diffusion in zircoloy-4 getter are available at www.osti.gov with https://doi.org/10.2172/2500850 and https://doi.org/10.2172/2279020. The VASP software can be found at https://www.vasp.at. The version of VASP employed for this study is 5.4.4.